Coulomb form factors of even-even nuclei described by axially deformed relativistic mean-field models

Jian Liu,[1,*] Chang Xu,[2] and Zhongzhou Ren[2]
[1]*College of Science, China University of Petroleum (East China), Qingdao 266580, China*
[2]*Department of Physics and Key Laboratory of Modern Acoustics, Nanjing University, Nanjing 210093, China*
(Received 24 January 2017; published 21 April 2017)

Background: Combining the relativistic mean-field (RMF) model and distorted wave Born approximation (DWBA) method, Coulomb form factors for elastic electron scattering have been studied for several stable nuclei (^{208}Pb, ^{40}Ca, ^{32}S, and ^{24}Mg) with a methodology that can be extended to exotic nuclei.
Purpose: Previous studies on nuclear Coulomb form factors by the RMF + DWBA method were mainly based on the spherical RMF model. This work aims to further extend the studies to the axially deformed RMF model.
Method: The nuclear proton density distributions are first calculated by the deformed RMF model. Next, the axially deformed density distributions are expanded into multipole components. With the spherical ρ_0 components, the Coulomb form factors of even-even nuclei are calculated by the DWBA method.
Results: For spherical nuclei, the nuclear Coulomb form factors obtained with the deformed RMF model almost coincide with those from the spherical RMF model. For deformed nuclei, Coulomb form factors obtained with the deformed RMF model agree better with the experimental data at the diffraction minima and at high momentum transfers.
Conclusions: Results indicate the proton densities calculated from the axially deformed RMF model are valid and reasonable. The electron-scattering experiments will soon be available for exotic nuclei, and the studies in this paper are helpful to interpret the experimental data of deformed exotic nuclei.

DOI: 10.1103/PhysRevC.95.044318

I. INTRODUCTION

Electron scattering provides an effective method to study the nuclear electromagnetic structure [1–6]. The interactions between the electrons and nucleons are mainly electromagnetic forces and the analysis of the experimental data does not involve theoretical uncertainties. In past decades, the electron-scattering experiments have been carried out for many stable nuclei. Assuming the target nuclei are spherically symmetric, their charge-density distributions can be extracted accurately from the electron-scattering experiments [7]. With the development of electron-scattering experiments, different theoretical methods have been developed to analyze the experimental Coulomb form factors, such as the plane-wave Born approximation (PWBA), the relativistic eikonal approximation [8], and the phase-shift analysis method [9–11]. The relativistic eikonal approximation and phase-shift analysis method can be referred to as the distorted-wave Born approximation (DWBA) [12] method because the nuclear Coulomb distortion effects are included.

Recently, the structure of exotic nuclei has become a focus research of nuclear physics [13,14], and it is valuable to explore the charge-density distributions of exotic nuclei by electron scattering [15–22]. To provide useful guides for the coming experiments, many theoretical researches have been done on the electron scattering off exotic nuclei in recent years. With the combination of the mean-field model and the DWBA method, the Coulomb form factors of unstable nuclei are systematically investigated [23–34], and many meaningful results are obtained. However, in previous studies, the target nuclei are usually seen as spherical. Most nuclei whose proton and neutron numbers are not magic numbers are deformed, as confirmed by many theoretical and experimental studies, such as, for example, the finite-range droplet model, self-consistent mean-field calculations, the extended Thomas–Fermi with Strutinsky integral model calculations, and $B(E2\uparrow)$ measurements [35–39]. Therefore, in this paper we use the deformed mean-field model instead of the spherical mean-field model to study the nuclear Coulomb form factors.

For the mean-field model, there are many choices for the effective interaction [40]; for example, the Gogny interaction [41] and Skyrme interactions [42,43]. Besides these nonrelativistic effective interactions, the relativistic mean-field model (RMF) is another method to deal with the nuclear many-body problems [44]. The spin degrees of freedom of nucleons in the RMF model are treated microscopically and the spin-orbit splitting is given automatically, since it is essentially a relativistic effect. It has been proved that RMF model can well describe the ground-state properties of finite nuclei in all mass regions with one parameter set [40]. Therefore, in this paper the deformed RMF model is chosen to obtain the nuclear ground-state properties; for example, the binding energies, charge radii, and deformations. Based on the results of deformed RMF model, we further carry out the DWBA calculations to investigate the nuclear Coulomb form factors.

By the combination of the deformed RMF model and DWBA method, the validity of the deformed RMF model can be tested by the electron-scattering experiments. In previous research, the experimental charge root mean square (rms) radii are usually used to check the theoretical results of deformed RMF model. However, one charge radius may correspond to

*liujian@upc.edu.cn

different charge-density distributions. This will add uncertainties to the theoretical results. Compared to the charge radius, the Coulomb form factor, which can be seen approximately as the Fourier transformation of the corresponding charge distribution, is unique for each charge distribution. Therefore, by the experimental Coulomb form factors obtained from the electron-scattering experiments, we can further examine the validity of the deformed RMF model with certain parameter set. In this paper, two well-calibrated parameter sets of RMF model are chosen for the discussion: one is the classical NL3 parameter set [45], which achieves enormous success in descriptions of the ground-state properties of many nuclei throughout the periodic table; another is the new FSUGarnet parameter set [46,47], which also displays the validity for the neutron-rich isotopes near the neutron drip lines. The proton density distributions of even-even nuclei are obtained by these two density functionals and the corresponding Coulomb form factors are investigated. By analyzing with both the spherical and deformed nuclei, the validity of the deformed RMF model are further examined by the experimental Coulomb form factors. The studies in this paper are also helpful for the analysis of the new scattering experimental data of deformed exotic nuclei.

The paper is organized as follows: In Sec. II, a brief review of the theoretical framework for the RMF model and DWBA method is provided. In Sec. III, numerical results and discussions are presented. Finally, a summary is given in Sec. IV.

II. THEORETICAL FRAMEWORK

In this section, we present the formalism for calculations of nuclear Coulomb form factors by the combination of the deformed RMF model and DWBA method. In the first part of this section, we introduce the axial deformation constrained RMF model. In the second part of this section, we discuss the DWBA method for calculating the Coulomb form factors of deformed even-even nuclei.

A. Axially deformed relativistic mean-field model

In the framework of RMF theory, the nuclear interaction is usually described by the exchange of mesons, and the effective Lagrangian density can be written in the following form [48]:

$$\begin{aligned}\mathcal{L} = \bar{\psi}\Big[\gamma^{\mu}\Big(i\partial\mu - g_{\omega}\omega_{\mu} - \frac{g_{\rho}}{2}\rho_{\mu}^{a}\tau^{a} - \frac{e}{2}(1+\tau^{3})A_{\mu}\Big) \\ -(M - g_{s}\sigma)\Big]\psi \\ +\frac{1}{2}\partial^{\mu}\sigma\,\partial_{\mu}\sigma - \frac{1}{2}m_{\sigma}^{2}\sigma^{2} - \frac{\kappa}{3!}(g_{s}\sigma)^{3} - \frac{\lambda}{4!}(g_{s}\sigma)^{4} \\ -\frac{1}{4}\Omega^{\mu\nu}\Omega_{\mu\nu} + \frac{1}{2}m_{\omega}^{2}\omega^{\mu}\omega_{\mu} + \frac{\xi}{4!}\big(g_{\omega}^{2}\omega^{\mu}\omega_{\mu}\big)^{2} \\ -\frac{1}{4}\vec{R}^{\mu\nu}\cdot\vec{R}_{\mu\nu} + \frac{1}{2}m_{\rho}^{2}\vec{\rho}^{\,\mu}\cdot\vec{\rho}_{\mu} \\ -\frac{1}{4}F^{\mu\nu}F_{\mu\nu} + U_{\text{eff}}(\omega_{\mu},\vec{\rho}^{\,\mu}),\end{aligned} \tag{1}$$

and the self-interacting term of nonlinear omega-rho coupling is taken as

$$U_{\text{eff}}(\omega_{\mu},\vec{\rho}^{\,\mu}) = \Lambda_{\text{v}}\big(g_{\rho}^{2}\vec{\rho}^{\,\mu}\vec{\rho}_{\mu}\big)\big(g_{\omega}^{2}\omega^{\mu}\omega_{\mu}\big). \tag{2}$$

With the Euler–Lagrange equation, the motion equations of nucleons can be derived. Based on the no-sea approximation and mean-field approximation, the Dirac equation of nucleons is written as

$$\{-i\boldsymbol{\alpha}\cdot\boldsymbol{\nabla} + \beta[M - S(\mathbf{r})] + U(\mathbf{r})\}\psi_{i}(\mathbf{r}) = \varepsilon_{i}\psi_{i}(\mathbf{r}), \tag{3}$$

where $S(\mathbf{r})$ and $U(\mathbf{r})$ are the scalar and vector potentials, respectively. From the effective Lagrangian density, the Klein–Gordon equations for the mesons and photon can also be obtained.

For axially symmetric deformed nuclei, the single-particle wave functions are characterized by the eigenvalue Ω_i of the third component of the total angular momentum j on the symmetry axis z, by the parity π_i, and by the z component of the isospin t_i. The spinor can be written in the form [49]

$$\psi_{i}(\mathbf{r},t) = \begin{pmatrix} f_{i}(\mathbf{r},s) \\ ig_{i}(\mathbf{r},s)\end{pmatrix}\chi_{t_{i}}(t). \tag{4}$$

Expanding the Dirac spinor with the eigenfunctions ϕ_α of an axially symmetric deformed harmonic-oscillator potential in cylindrical coordinates, we can obtain

$$\begin{aligned} f_{i}(\mathbf{r},s,t) &= \frac{1}{\sqrt{2\pi}}\begin{pmatrix} f_{i}^{+}(z,r_{\perp})e^{i(\Omega-1/2)\pi} \\ f_{i}^{-}(z,r_{\perp})e^{i(\Omega+1/2)\pi}\end{pmatrix} \\ &\quad\times\sum_{\alpha}^{\alpha_{\max}} f_{\alpha}^{(i)}\Phi_{\alpha}(\mathbf{r},s)\chi_{t_{i}}(t), \\ g_{i}(\mathbf{r},s,t) &= \frac{1}{\sqrt{2\pi}}\begin{pmatrix} g_{i}^{+}(z,r_{\perp})e^{i(\Omega-1/2)\pi} \\ g_{i}^{-}(z,r_{\perp})e^{i(\Omega+1/2)\pi}\end{pmatrix} \\ &\quad\times\sum_{\tilde{\alpha}}^{\tilde{\alpha}_{\max}} g_{\tilde{\alpha}}^{(i)}\Phi_{\tilde{\alpha}}(\mathbf{r},s)\chi_{t_{i}}(t), \end{aligned} \tag{5}$$

where Φ_α can be expressed in terms of Hermite and Laguerre polynomials.

Substituting Eqs. (4) and (5) into the Dirac equation (3), the coefficients $f_{\alpha}^{(i)}$ and $g_{\tilde{\alpha}}^{(i)}$ can be obtained. Combining the Klein–Gordon equations of mesons, the Dirac equations can be solved by iterations. After the Dirac spinors of nucleons are obtained, we can calculate the binding energies, charge rms radii, nuclear quadrupole moments, and proton density distributions.

B. Nuclear Coulomb form factors

For the deformed density distribution calculated from the axially deformed RMF model, it can be expanded in multipoles by the Legendre function [50]:

$$\begin{aligned}\rho(r,z) &= \sum_{k}\rho_{k}(R)P_{k}(\cos\theta) \\ &= \rho_{0}(R) + \rho_{2}(R)P_{2}(\cos\theta) + \cdots,\end{aligned} \tag{6}$$

where the multipole components can be written as

$$\rho_k(R) = \frac{2k+1}{2}\int_{-1}^{1} P_k(\cos\theta)\rho(R\cos\theta, R\sin\theta)d(\cos\theta). \quad (7)$$

In PWBA method, the proton form factor is defined as the Fourier transformation of the proton distribution:

$$F_p(q) = \frac{1}{Z}\int \rho_p(\vec{r})e^{i\vec{q}\cdot\vec{r}}d\vec{r}, \quad (8)$$

where the exponential function $e^{i\vec{q}\cdot\vec{r}}$ can be expanded as partial waves:

$$e^{i\vec{q}\cdot\vec{r}} = \sum_{\lambda}^{\infty} i^{\lambda}(2\lambda+1)j_\lambda(qr)P_\lambda(\cos\theta). \quad (9)$$

Substituting Eq. (6) into Eq. (8) and taking into account of the relations between the intrinsic multipoles and Coulomb multipoles, the proton form factor can be decomposed into several multipoles by selection rules [51]:

$$|F_p(q)|^2 = \sum_{\lambda=0,2,\ldots} |C_\lambda(q)|^2. \quad (10)$$

For each multipole λ, the C_λ form factor is defined as

$$C_\lambda(q) = \frac{1}{Z}\int d^3r\rho_\lambda(r)j_\lambda(qr), \quad (11)$$

where $\rho_\lambda(r)$ is the λ order multipole component of the deformed proton density.

Folding the proton form factor with the electric form factor of a single proton $G_E(q)$ [52] and taking into account the center-of-mass correction $F_{\text{c.m.}}(q)$ [53], we can obtain the nuclear Coulomb form factor:

$$F_C(q) = F_p(q)G_E^p(q)F_{\text{c.m.}}(q). \quad (12)$$

For elastic electron scattering off nuclei with angular momentum $J^\pi = 0^+$, only the C_0 multipole exists in the longitudinal form factor by the angular-momentum considerations. From Eqs. (10) and (12), the C_0 multipole is attributed to the spherical part $\rho_0(r)$ of the proton density. Therefore, for elastic electron scattering off deformed even-even nuclei, only the $\rho_0(r)$ contributes to the total Coulomb form factor.

The Coulomb form factor of the Eq. (11) is performed with the plane-wave description, where the nuclear Coulomb distortion effects are neglected. To obtain more accurate results, the DWBA method are needed where the Coulomb distortions are included. In this paper, an approximate method is used to deal with the the nuclear Coulomb distortion effects. If the nuclear deformation is not large, we neglect Coulomb distortions of the aspherical parts and only include the Coulomb distortions of the spherical part of $\rho_0(r)$. By this way, the C_0 multipole, which is the major component of the Coulomb form factor, is calculated with the full DWBA method. At this case, the Coulomb potential $V(r)$ for large r is also Z/r as it should be, because

$$\int_V [\rho_0(r) + \rho_2(r)P_2(\cos\theta) + \cdots]d^3r = \int_V \rho_0(r)d^3r = Z. \quad (13)$$

TABLE I. Theoretical binding energies per nucleon B/A (MeV), charge rms radii R_C (fm), neutron skins R_{np} (fm), and deformation parameter β_2 for some spherical and deformed nuclei, calculated by the axially deformed RMF model with NL3 and FSUGarnet parameter sets. The experimental data are taken from the Refs. [36,55,56]. In the table, FSUGarnet is abbreviated as FSUG.

Nuclei	Forces	B/A	R_C	β_2	R_{np}
^{208}Pb	NL3	7.88	5.51	−0.004	0.28
	FSUG	7.91	5.49	0.000	0.16
	Expt.	7.87	5.50	0.055	
^{40}Ca	NL3	8.59	3.49	0.000	−0.06
	FSUG	8.53	3.47	−0.006	−0.07
	Expt.	8.55	3.48	0.123	
^{32}S	NL3	8.30	3.29	0.198	−0.06
	FSUG	8.33	3.25	0.134	−0.06
	Expt.	8.49	3.26	0.312	
^{24}Mg	NL3	8.06	3.15	0.440	−0.05
	FSUG	8.08	3.12	0.427	−0.06
	Expt.	8.26	3.06	0.605	

A similar method has been used in Ref. [52] to investigate the Coulomb form factor of ^{27}Al. With this approximation, we can do the DWBA calculations by numerically solving the Dirac equation and summing partial waves.

In DWBA method, the elastic electron scattering by the nuclear electrostatic potential is described by the Dirac equation [54]:

$$[\boldsymbol{\alpha}\cdot\boldsymbol{p} + \beta m + V(\mathbf{r})]\Psi(\mathbf{r}) = E\Psi(\mathbf{r}), \quad (14)$$

where $V(\mathbf{r})$ is the Coulomb potential of the spherical part $\rho_0(r)$ of the deformed proton densities. The wave functions of scattered electrons can be expanded in terms of spherical spinors with definite angular momentum:

$$\Psi(\mathbf{r}) = \frac{1}{r}\begin{bmatrix} P(r)\Omega_{\kappa,m_j}(\theta,\phi) \\ iQ(r)\Omega_{-\kappa,m_j}(\theta,\phi)\end{bmatrix}. \quad (15)$$

The upper component $P(r)$ and lower component $Q(r)$ of the radial wave function at large distances can be determined with the phase shift δ. Substituting Eq. (15) into Eq. (14), the spin-up δ_l^+ and spin-down δ_l^- phase shifts for the partial wave with orbital angular momentum l can be solved. With the phase shifts of the wave functions, the direct scattering amplitude and

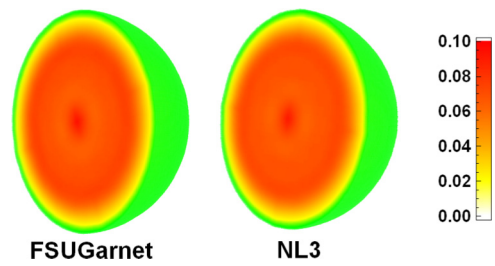

FIG. 1. Ground-state proton densities (units of fm^{-3}) and nuclear surface shapes of ^{208}Pb, calculated by the deformed RMF model with FSUGarnet and NL3 parameter sets.

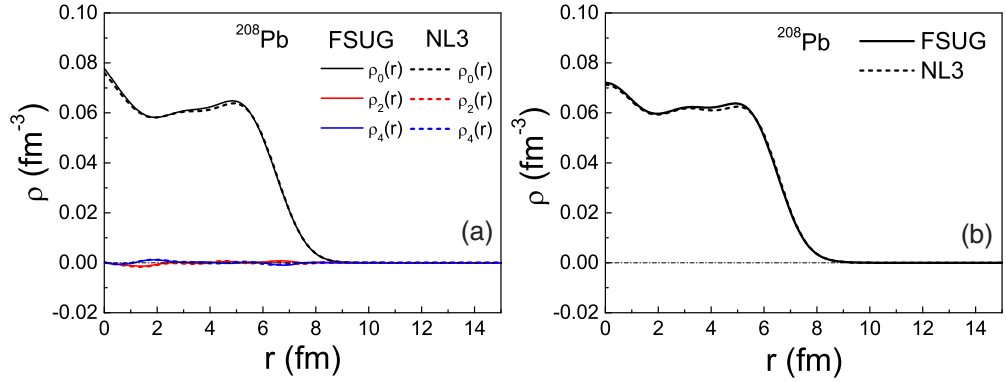

FIG. 2. (a) The density multipole components of ^{208}Pb for deformed proton distributions in Fig. 1, which are obtained by Eqs. (6) and (7). (b) The proton distributions of ^{208}Pb, calculated by the spherical RMF model. In the figure, FSUGarnet is abbreviated as FSUG.

spin-flip scattering amplitude can be determined as [32]

$$f(\theta) = \frac{1}{2ik}\sum_{l=0}^{\infty}\left[(l+1)(e^{2i\delta_l^+}-1)+(e^{2i\delta_l^-}-1)\right]P_l(\cos\theta),$$

$$g(\theta) = \frac{1}{2ik}\sum_{l=0}^{\infty}\left[e^{2i\delta_l^-}-e^{2i\delta_l^+}\right]P_l^1(\cos\theta), \tag{16}$$

with P_l and P_l^1 denoting the Legendre and associated Legendre function. The electron-scattering amplitudes $f(\theta)$ and $g(\theta)$ are given as sum of infinite partial waves. However, their Legendre expansion has fast convergence with l increasing. For electron scattering off the heavy nucleus ^{208}Pb with incident energy 600 MeV, about 40 partial waves need to be taken into account in numerical calculations. For light nuclei such as Ca and S, the numbers of partial waves required are fewer. When the scattering amplitudes $f(\theta)$ and $g(\theta)$ are obtained, the C_0 multipole can be calculated as

$$F_{C_0}(q) = \left(|f(\theta)|^2 + |g(\theta)|^2\right)/\sigma_{\text{Mott}}, \tag{17}$$

where the Mott scattering cross section is

$$\sigma_M(\theta) = \left(\frac{Z\alpha}{2E}\right)^2 \frac{\cos^2\frac{1}{2}\theta}{\sin^4\frac{1}{2}\theta}. \tag{18}$$

III. NUMERICAL RESULTS AND DISCUSSION

With the formula presented in Sec. II, the Coulomb form factors are calculated in this section for both the spherical and deformed even-even nuclei. By comparing the theoretical results with the experimental data, the validity of the axially deformed RMF model is examined. The nuclear proton densities are calculated under the deformed RMF models with two parameter sets. One is the NL3 parameter set [45], which provides many descriptions for nuclei throughout the periodic table. The other is the new calibrated FSUGarnet parameter set [46,47], which displays a soft symmetry energy and provides good descriptions for nuclei near the neutron trip line.

In Table I, we present the theoretical binding energies per nucleon B/A, charge rms radii R_C, neutron skins $R_{np} = R_n - R_p$, and deformation parameter β_2 for both the spherical and deformed nuclei, which are calculated by the axially deformed RMF model with the NL3 and FSUGarnet parameter sets, respectively. The experimental data are also given in this table. From this table, it can be seen that the theoretical results agree with the experimental data for these two parameter sets. However, the charge rms radii R_C only provide a rough description for the nuclear ground-state properties, because different density distributions can correspond to the same rms radii. Compared with charge rms radii R_C, the Coulomb form factor can provide a better description for the nuclear

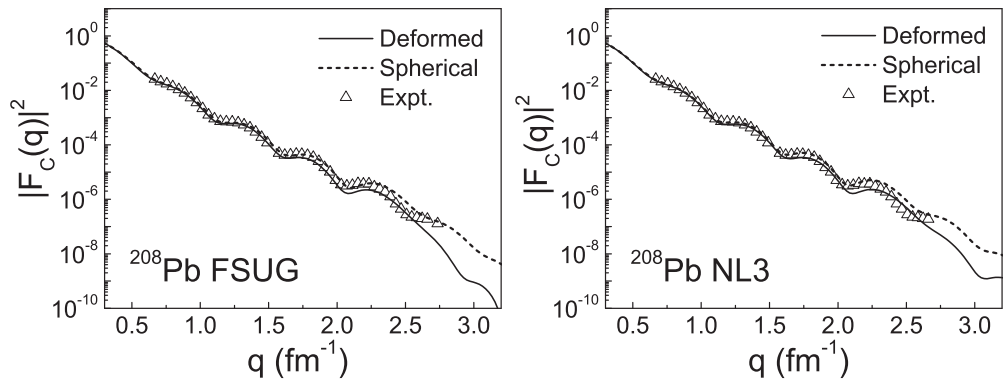

FIG. 3. Nuclear Coulomb form factors of ^{208}Pb, where the corresponding proton density distributions are calculated by the spherical RMF model and axially deformed RMF model with two parameter sets, respectively. In the figure, FSUGarnet is abbreviated as FSUG.

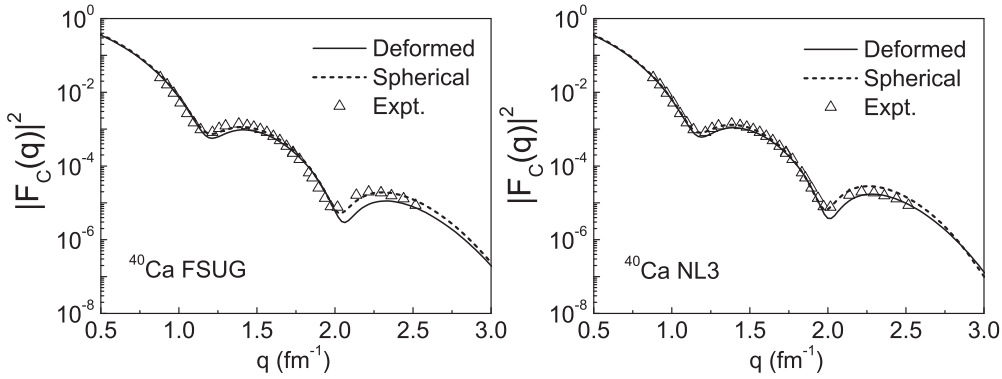

FIG. 4. Nuclear Coulomb form factors of ^{40}Ca, where the corresponding proton density distributions are calculated by the spherical RMF model and axially deformed RMF model with two parameter sets, respectively. In the figure, FSUGarnet is abbreviated as FSUG.

electromagnetic properties. Therefore, the theoretical nuclear Coulomb form factors for nuclei in Table I are investigated by the DWBA method.

A. Spherical nuclei

First, the Coulomb form factors of spherical nuclei are investigated by the deformed RMF model and DWBA method. The double magic nuclei ^{208}Pb and ^{40}Ca always serve as a benchmark for studying the nuclear properties. Therefore, Coulomb form factors of ^{208}Pb and ^{40}Ca are an important examination for the recent research. The ground-state proton density distributions of ^{208}Pb calculated by the deformed RMF model with different parameter sets are presented in Fig. 1, and the corresponding density multipole components for the deformed proton distributions are given in Fig. 2(a). As a comparison, the proton densities calculated by the spherical RMF model are presented in Fig. 2(b). In these two figures, one can see that the proton density distributions of ^{208}Pb calculated from the deformed RMF model have a spherical surface shape, and the deformed multipole components ρ_2 and ρ_4 are very close to zero.

With the spherical multipole components ρ_0 in Fig. 2(a), the Coulomb form factors of ^{208}Pb are calculated by the DWBA method, and the results are presented in Fig. 3. From this figure, one can see that, for ^{208}Pb, the Coulomb form factors from the deformed RMF proton densities coincide with those from the spherical RMF densities, and both of them have good agreements with the experimental data. Only at high momentum transfers ($q > 2.8$ fm^{-1}), a small deviation occurs between the results of deformed RMF model and spherical RMF model, and there are no experimental data in this range. The form factors at high momentum transfers are mainly sensitive to the inner parts of the density distributions. Therefore, further experiments at high momentum transfers will be helpful to constrain the central density distribution of ^{208}Pb. Results in Fig. 3 indicate that for the spherical nucleus ^{208}Pb, the deformed RMF model can also give an effective description for its proton density distributions.

Besides ^{208}Pb, the Coulomb form factors of ^{40}Ca are also investigated with the deformed RMF model and DWBA method. In Table I, charge rms radii of ^{40}Ca are calculated by the deformed RMF model with FSUGarnet and NL3 parameter sets, and the results coincide with the experimental data. Besides the charge rms radii, the nuclear Coulomb form factors for the deformed RMF proton densities of ^{40}Ca are further calculated and presented in Fig. 4. In this figure, the theoretical Coulomb form factors from the deformed RMF model have good agreement with the experimental data and Coulomb form factors of the spherical RMF model. Combining Figs. 2–4, one can see that, for the spherical nuclei, the proton density distributions obtained from the deformed RMF model are consistent with those from the spherical RMF model. This is because, for spherical nuclei, the deformed RMF programs also converge to the case of the spherical solutions. The deformed RMF model is more general and contains the solutions for the spherical nuclei.

B. Deformed nuclei

Besides the spherical nuclei, the Coulomb form factors of deformed nuclei in Table I are also investigated in this paper. In Fig. 5, the ground-state proton density distributions of ^{32}S are presented, which are calculated by the deformed RMF model with the FSUGarnet and NL3 parameter sets. From this figure, it can be seen that the RMF proton density distributions from different parameter sets are very similar. Both of them have a prolate shape, and their density distributions are depressed in the center because of the lower population of s-wave orbitals. There are also small differences between the results of FSUGarnet and NL3 parameter sets. The central proton

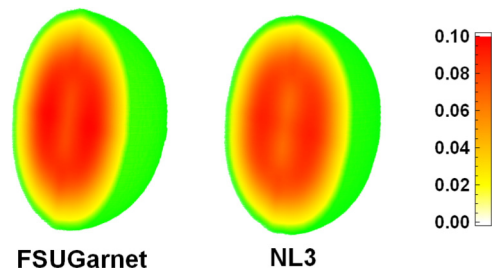

FIG. 5. Ground-state proton densities (units of fm^{-3}) and nuclear surface shapes of ^{32}S, calculated by the deformed RMF model with FSUGarnet and NL3 parameter sets.

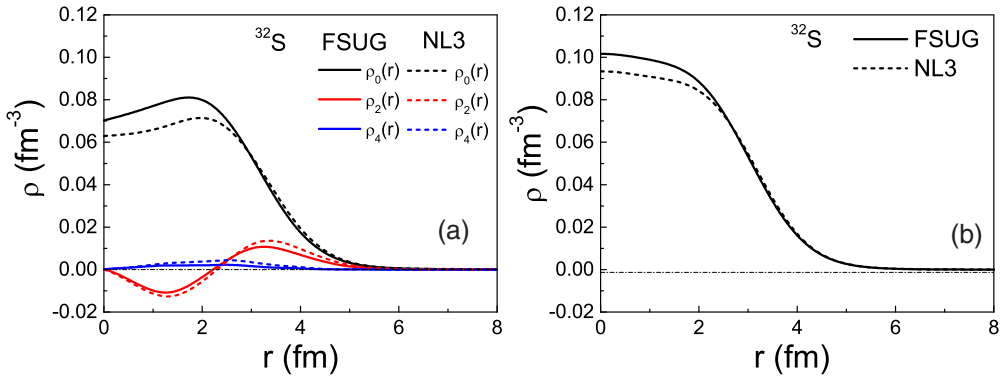

FIG. 6. (a) The density multipole components for deformed proton distributions of ^{32}S in Fig. 5, which are obtained by Eqs. (6) and (7). (b) The proton density distributions of ^{32}S, calculated by the spherical RMF model. In the figure, FSUGarnet is abbreviated as FSUG.

density distribution from the NL3 parameter set is smaller than that from the FSUGarnet set.

With Eqs. (6) and (7), the proton distributions in Fig. 5 are further decomposed into different multipole components. The multipole components ρ_0, ρ_2, and ρ_4 for the deformed RMF proton densities of ^{32}S are presented in Fig. 6(a). For comparison, the proton density distributions of ^{32}S calculated by the spherical RMF model are also presented in Fig. 6(b). Although ^{32}S is a deformed nucleus, the spherical part ρ_0 is still the major part of its proton distributions. The multipole ρ_2 provides the nuclear quadruple deformation, which is much smaller than ρ_0. With the multipole order k increasing, the values of the components decrease very rapidly. In Fig. 6(a), for multipoles ρ_k ($k \geqslant 4$), its contributions to the proton densities can be neglected. To study the Coulomb form factors of even-even nucleus ^{32}S, only the spherical part ρ_0 need to be taken into account.

The nuclear Coulomb form factors of ^{32}S for deformed RMF proton density distributions in Fig. 5 are investigated with the formulas in Sec. II, and the results are presented in Fig. 7. For comparison, the Coulomb form factors of the spherical RMF proton density distributions are also calculated and presented in Fig. 7. From this figure, one can see that the Coulomb form factors calculated from the spherical and deformed models are very close to each other. Both of them can describe the experimental data. At the first diffraction minimum ($q \simeq 1.2$ fm^{-1}), there are small discrepancies between the experimental data and theoretical results of the spherical RMF model. The Coulomb form factors calculated from the deformed RMF model coincide with the experimental data better at the first diffraction minimum. Results in Fig. 7 show the proton density distributions of ^{32}S from the axially deformed RMF models are valid and reasonable.

Besides the ^{32}S, the Coulomb form factors of ^{24}Mg are also investigated with the deformed RMF model and DWBA method. In Fig. 8, we present the ground-state proton density distributions and nuclear surface shapes of ^{24}Mg, which are calculated by the axially deformed RMF model with the FSUGarnet and NL3 parameter sets, respectively. Compared with Fig. 5, one can see that there are also central depression in the proton density distributions of ^{24}Mg because of the lower population of s-wave orbitals. Besides the central depression, there are two regions of pronounced localization at the outer ends of the symmetry axis. The density multipole components ρ_k for the deformed RMF proton distributions of ^{24}Mg in Fig. 8 are also calculated by Eqs. (6) and (7), and the results are presented in Fig. 9(a). In Fig. 9(b), we also provide the proton densities of ^{24}Mg, which are calculated by the spherical RMF model. From Fig. 9, one can see that the quadrupole components ρ_2 of proton density distributions of ^{24}Mg are larger than those of ^{32}S, which can interpret the larger deformation parameter β_2 of ^{24}Mg in Table I.

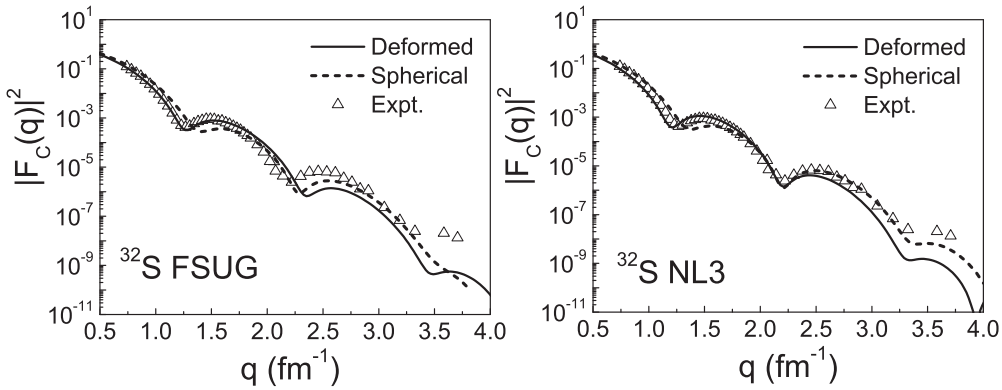

FIG. 7. Nuclear Coulomb form factors of ^{32}S, where the corresponding proton density distributions are calculated by the spherical RMF model and axially deformed RMF model with two parameter sets, respectively. In the figure, FSUGarnet is abbreviated as FSUG.

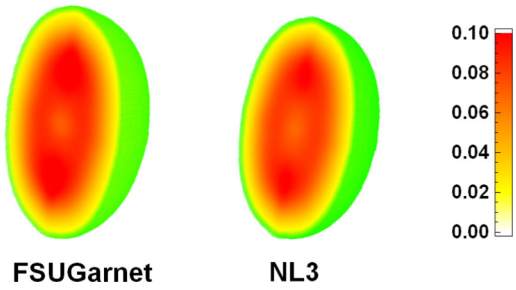

FIG. 8. Ground-state proton densities (units of fm^{-3}) and nuclear surface shapes of ^{24}Mg, calculated by the deformed RMF model with FSUGarnet and NL3 parameter sets.

With the spherical components ρ_0 in Fig. 9, the Coulomb factors of ^{24}Mg are calculated, and the results are presented in Fig. 10. From two panels of Fig. 10, one can see that the theoretical Coulomb factors from the deformed RMF model present good agreements with the experimental data. Especially in the range of high momentum transfers ($q > 2$ fm^{-1}), there are deviations between the theoretical results of spherical RMF model and experimental data. However, the results of the deformed RMF model coincide with the experimental data better in this range. The form factors in high momentum transfers are sensitive to the details of the inner part of density distributions. Therefore, results in Fig. 10 indicate that for ^{24}Mg, the deformed RMF model can give a better descriptions on the density distributions at the central part of the nucleus, compared with the spherical RMF model.

IV. SUMMARY

The nuclear Coulomb form factors are important quantities, which can accurately reflect the nuclear electromagnetic structure. In previous theoretical studies, the combination of the spherical RMF model and DWBA method was widely used to study the nuclear Coulomb form factors. The purpose of this paper is to extend this method to the deformed RMF model. In this paper, the Coulomb form factors of even-even nuclei are systematically investigated by the deformed RMF model and the DWBA method.

For even-even nuclei, the Coulomb form factors only contain the C_0 multipoles by the angular-momentum consideration. The C_0 multipole is attributed to the spherical part of the proton distribution. Therefore, we first calculate the nuclear proton density by the deformed RMF model. Next, the RMF proton distribution is expanded in multipoles by the Legendre function to extract its spherical part $\rho_0(r)$. After the $\rho_0(r)$ is obtained, the C_0 multipole is studied with the DWBA method. An approximate method is used to deal with the nuclear Coulomb distortion effects. If the nuclear deformation is not large, we neglect the Coulomb distortions of the aspherical parts and do the DWBA calculations where only the Coulomb distortions of spherical parts $\rho_0(r)$ are taken into account.

During the studies, both the spherical and deformed nuclei are chosen as the candidates. Their density distributions are calculated by the axially deformed RMF model with two parameter sets. One is the classical NL3 parameters and the other is the new FSUGarnet parameters. The Coulomb form factors of these nuclei are investigated and the results are compared with the experimental data. For spherical nuclei, the theoretical Coulomb form factors from the deformed RMF models almost coincide with those from the spherical RMF models, and both of them have good agreement with the experimental data. For deformed nuclei, the Coulomb form factors calculated from deformed RMF model modify the results of spherical RMF model at the diffraction minima and at high momentum transfers. Results in this paper indicate that deformed RMF model contains the solutions for the spherical nuclei and also provide better descriptions for the deformed nuclei. The new experiments of elastic electron scattering off exotic nuclei are under way. The studies in this paper are also helpful to interpret the experimental data of electron scattering off exotic deformed nuclei.

ACKNOWLEDGMENTS

The authors are grateful to Xavier Roca–Maza for valuable discussions and careful reading of the manuscript. This work is supported by the National Natural Science Foundation of China (Grants No. 11505292, No. 11575082, No. 11235001, No. 11605105, and No. 11275138), by the Shandong Provincial Natural Science Foundation, China (Grant

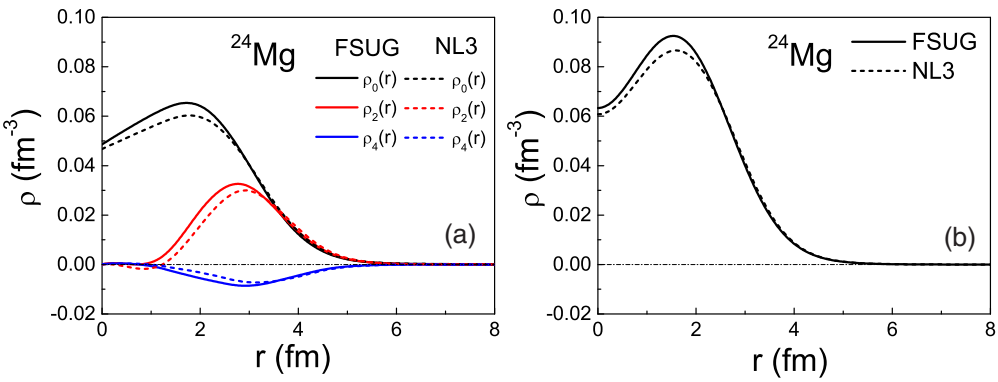

FIG. 9. (a) The density multipole components of ^{24}Mg for deformed proton distributions in Fig. 8, which are obtained by Eqs. (6) and (7). (b) The proton densities of ^{24}Mg, calculated by the spherical RMF model. In the figure, FSUGarnet is abbreviated as FSUG.

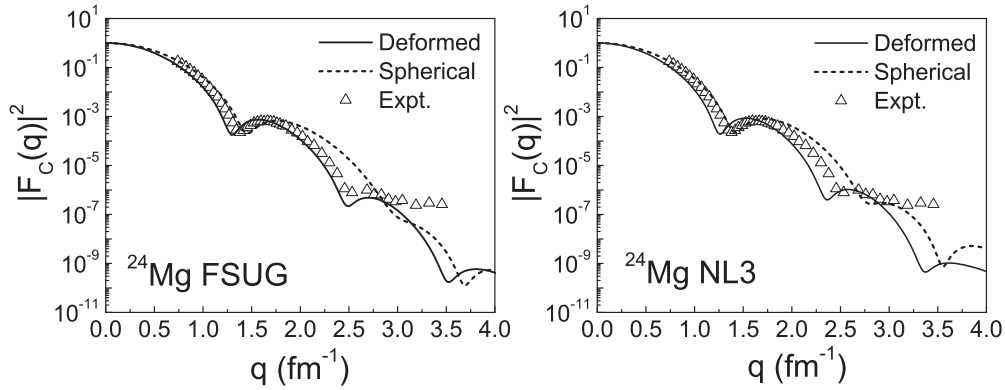

FIG. 10. Nuclear Coulomb form factors of ^{24}Mg, where the corresponding proton density distributions are calculated by the spherical RMF model and axially deformed RMF model with two parameter sets, respectively. In the figure, FSUGarnet is abbreviated as FSUG.

No. BS2014SF007), by the Fundamental Research Funds for the Central Universities (Grant No. 17CX02044), and by the International S&T Cooperation Program of China (Grant No. 2016YFE0129300).

[1] I. Sick and D. Trautmann, Phys. Rev. C **89**, 012201 (2014).
[2] R. Hofstadter, Rev. Mod. Phys. **28**, 214 (1956).
[3] R. S. Willey, Nucl. Phys. **40**, 529 (1963).
[4] T. de Forest and J. D. Walecka, Adv. Phys. **15**, 1 (1966).
[5] Herbert Überall, *Electron Scattering from Complex Nuclei* (Academic Press, New York, London, 1971).
[6] John Dirk Walecka, *Electron Scattering for Nuclear and Nucleon Structure* (Cambridge University Press, Cambridge, 2001).
[7] H. De Vries, C. W. De Jager, and C. De Vries, At. Data Nucl. Data Tables **36**, 495 (1987).
[8] A. Baker, Phys. Rev. **134**, B240 (1964).
[9] D. Yennie, F. Boos, and D. Ravenhall, Phys. Rev. **137**, B882 (1965).
[10] J. Heisenberg, Adv. Nucl. Phys. **12**, 1 (1981).
[11] M. Nishimura, E. Moya De Guerra, D. W. L. Sprung, Nucl. Phys. A **435**, 523 (1985).
[12] D. H. Jakubassa-Amundsen, J. Phys. G **41**, 075103 (2014).
[13] I. Tanihata, Prog. Part. Nucl. Phys. **35**, 505 (1995).
[14] A. C. Mueller, Prog. Part. Nucl. Phys. **46**, 359 (2001).
[15] E. Garrido and E. Moya de Guerra, Nucl. Phys. A **650**, 387 (1999).
[16] E. Moya de Guerra, E. Garrido, and P. Sarriguren, *Challenges in Nuclear Structure, Proceedings of the 7th International Spring Seminar on Nuclear Physics* (World Scientific Publishing Co., 2002).
[17] A. N. Antonov *et al.*, Nucl. Instrum. Methods Phys. Res., Sect. A **637**, 60 (2011).
[18] M. Wakasugi *et al.*, Phys. Rev. Lett. **100**, 164801 (2008).
[19] T. Suda *et al.*, Phys. Rev. Lett. **102**, 102501 (2009).
[20] T. Suda, J. Phys.: Conf. Ser. **267**, 012008 (2011).
[21] T. Suda and M. Wakasugi, Prog. Part. Nucl. Phys. **55**, 417 (2005).
[22] H. Simon, Nucl. Phys. A **787**, 102 (2007).
[23] Z. Wang and Z. Ren, Phys. Rev. C **70**, 034303 (2004).
[24] A. N. Antonov, D. N. Kadrev, M. K. Gaidarov, E. Moya de Guerra, P. Sarriguren, J. M. Udias, V. K. Lukyanov, E. V. Zemlyanaya, and G. Z. Krumova, Phys. Rev. C **72**, 044307 (2005).
[25] K. S. Jassim, A. A. Al-Sammarrae, F. I. Sharrad, and H. A. Kassim, Phys. Rev. C **89**, 014304 (2014).
[26] T. Dong, Z. Ren, and Y. Guo, Phys. Rev. C **76**, 054602 (2007).
[27] C. Zhang, J. Liu, and Z. Ren, J. Phys. G **43**, 045103 (2016).
[28] J. Liu, X. Zhang, C. Xu, and Z. Ren, Nucl. Phys. A **948**, 46 (2016).
[29] Y. Chu, Z. Ren, Z. Wang, and T. Dong, Phys. Rev. C **82**, 024320 (2010).
[30] Z. Wang, Z. Ren, and Y. Fan, Phys. Rev. C **73**, 014610 (2006).
[31] S. Karataglidis and K. Amos, Phys. Lett. B **650**, 148 (2007).
[32] X. Roca-Maza, M. Centelles, F. Salvat, and X. Viñas, Phys. Rev. C **78**, 044332 (2008).
[33] G. Gosselin, N. Pillet, V. Méot, P. Morel, and A. Y. Dzyublik, Phys. Rev. C **79**, 014604 (2009).
[34] X. Roca-Maza, M. Centelles, F. Salvat, and X. Viñas, Phys. Rev. C **87**, 014304 (2013).
[35] P. Moller, J. R. Nix, W. D. Myers, and W. J. Swiatecki, At. Data Nucl. Data Tables **59**, 185 (1995).
[36] S. Raman, C. W. Nestor, and P. Tikkanen, At. Data Nucl. Data Tables **78**, 1 (2001).
[37] N. J. Stone, At. Data Nucl. Data Tables **90**, 75 (2005).
[38] G. Scamps, D. Lacroix, G. G. Adamian, and N. V. Antonenko, Phys. Rev. C **88**, 064327 (2013).
[39] Y. Aboussir, J. M. Pearson, A. K. Dutta, and F. Tondeur, At. Data Nucl. Data Tables **61**, 127 (1995).
[40] M. Bender, P. H. Heenen, and P. G. Reinhard, Rev. Mod. Phys. **75**, 121 (2003).
[41] J. Decharge and D. Gogny, Phys. Rev. C **21**, 1568 (1980).
[42] D. Vautherin, Phys. Rev. C **5**, 626 (1972).
[43] D. Vautherin, Phys. Rev. C **7**, 296 (1973).
[44] P. Ring, Prog. Part. Nucl. Phys. **37**, 193 (1996).
[45] G. A. Lalazissis, J. Konig, and P. Ring, Phys. Rev. C **55**, 540 (1997).
[46] C. Chen and J. Piekarewicz, Phys. Lett. B **748**, 284 (2015).
[47] R. Utama, W.-C. Chen, and J. Piekarewicz, J. Phys. G **43**, 114002 (2016).
[48] B. G. Todd-Rutel and J. Piekarewicz, Phys. Rev. Lett. **95**, 122501 (2005).
[49] L. S. Geng, H. Toki, S. Sugimoto, and J. Meng, Prog. Theor. Phys. **110**, 921 (2003).

[50] E. Moya de Guerra, P. Sarriguren, and J. A. Caballero, Nucl. Phys. A **529**, 68 (1991).
[51] E. Moya de Guerra, Phys. Rep. **138**, 293 (1986).
[52] C. J. Horowitz, Phys. Rev. C **89**, 045503 (2014).
[53] B. A. Brown, R. A. Radhi, and B. H. Wildenthal, Phys. Rep. **101**, 313 (1983).
[54] D. Yennie, Phys. Rev. **95**, 500 (1954).
[55] M. Wang, G. Audi, A. H. Wapstra, F. G. Kondev, M. MacCormick, X. Xu, and B. Pfeiffer, Chin. Phys. C **36**, 1603 (2012).
[56] I. Angeli and K. P. Marinova, At. Data Nucl. Data Tables **99**, 69 (2013).